ELSEVIER

Chemical Engineering Journal 67 (1997) 153–166

Chemical Engineering Journal

The Kenics static mixer: a three-dimensional chaotic flow

D.M. Hobbs, F.J. Muzzio *

Department of Chemical and Biochemical Engineering, Rutgers University, P.O. Box 909, Piscataway, NJ 08855, USA

Received 6 June 1996; revised 10 January 1997; accepted 3 February 1997

Abstract

The Kenics static mixer was investigated numerically using Lagrangian methods to characterize mixer performance for low Reynolds number flows. Particle tracking simulations were used to compute residence time distributions, striation evolution, and variation coefficient as a function of the number of mixer elements. The mixing measures calculated from the numerical simulation agree closely with reported experimental results from the literature. Stretching of material elements in the mixer flow was also computed. The average stretching of material elements increased exponentially with the number of periodic mixer segments (a signature of chaotic flows). The probability density function of the logarithm of stretching values, $H_n(\log_{10}\lambda)$, had a Gaussian distribution over the central spectrum of stretching intensities, with no deviations from the Gaussian profile at low stretching intensities, suggesting a globally chaotic flow. A significant tail of high stretching intensities was found. The spatial locations of points with the highest stretching values corresponded to the manifolds of two period-1 hyperbolic points present in the flow. © 1997 Published by Elsevier Science S.A.

Keywords: Kenics static mixer; Three-dimensional chaotic flow

1. Introduction

Mixing is ubiquitous and essential in many facets of the chemical process industries, ranging from simple blending to complex chemical reactions for which the reaction yield and selectivity are highly dependent on the mixing performance. Improper mixing can result in non-reproducible processing and lowered product quality, with the associated need for more elaborate downstream purification processes and increased waste disposal costs. However, despite its importance, mixing performance is rarely characterized rigorously for industrial systems. Detailed characterizations are important, particularly in slow moving, high viscosity, laminar flows, which have a significant potential to lead to inhomogeneity and poorly mixed regions within the flow system.

Significant advances have been made in the study of fluid mechanical mixing using tools from dynamical systems theory, particularly those applying to chaos. Several experimental and computational studies of chaotic flows have been conducted to investigate the convection of passive tracers in such flow systems [1–3]. The majority of such studies have focused on two-dimensional, time periodic flows and have demonstrated that the evolution of partially mixed structures in a fluid system can be described based on the stretching and stirring of fluid elements placed into the flow [4–6]. The stretching distributions have also been related to the rate of intermaterial area generation and the striation thickness distributions obtained in the flow. A much smaller set of studies have investigated simple, three-dimensional, spatially periodic flows [7,8] where an analytical approximation to the velocity field could be obtained. Thus far, however, these powerful analysis tools have only been applied to idealized flow systems and have not been used to investigate a realistic, three-dimensional, industrially practical system.

The complex, three-dimensional geometries and flow fields typical of most industrial systems make analytic solutions for the velocity field impractical. However, for laminar flows, a high quality numerical solution of the velocity field can provide a starting point to characterize mixing performance. The use of commercially available computational fluid dynamics (CFD) software packages to solve fluid dynamics problems has become widespread in a number of disciplines. Such an approach will be adopted here to obtain a discrete approximation to the velocity field in an industrial mixing device, the Kenics mixer manufactured by Chemineer (Dayton, OH). Fig. 1 illustrates the standard configuration for this mixer. Each element of the Kenics mixer is a plate which has been given a 180° helical twist. The complete mixer consists of a series of elements of alternating clockwise and counterclockwise twist arranged axially within a tube so that the

* Corresponding author. Tel: +1 908 445 3357; fax: +1 908 445 5313; e-mail: muzzio@sol.rutgers.edu

PII S1385-8947(97)00013-2

leading edge of an element is at right angles to the trailing edge of the previous element. Laminar flow in the Kenics mixer is fully three-dimensional and spatially periodic in the axial direction, with each pair of adjacent elements forming a single periodic unit. For steady-state operation, the periodic spatial dimension in this flow is analogous to the periodic time dimension in previously studied two-dimensional flows.

A previous communication [9] described the three-dimensional velocity field in the Kenics mixer and characterized different regions of the flow based on profiles of the magnitudes of the rate-of-strain tensor, elongation velocity, and strain velocity. Such Eulerian measures provided a starting point for identifying the flow regions that potentially contribute the most to overall mixing performance, but they fail to capture the dynamics of the mixing process. A more complete analysis of mixing behavior requires the use of mixing measures based in the Lagrangian reference frame of the flowing fluid. In this paper, the evolution of fluid mixing is characterized using tracers that are convected by the flow field, providing a true Lagrangian characterization of mixing.

The remainder of this paper describes the tracking techniques and the results obtained from such computations. The fully three-dimensional velocity field for a Kenics mixer under laminar flow conditions is described in Section 2.1. Particle tracking software that is used to track the position of tracer particles as they are convected by the flow is described in Section 2.2. Tracking simulations involving a large number of tracer particles ($O(10^4)$) are used to describe mixing in the Kenics mixer in terms of residence time distributions (Section 3.1), striation development (Section 3.2), and variation coefficient vs. mixer length (Section 3.3). The tracking software is also used to compute the stretching of fluid elements. Mixing performance is then evaluated using tools that have been developed to analyze mixing in chaotic flows: stretching distributions, structure of the stretching field, and manifolds of periodic points (Section 3.4).

2. Algorithms

2.1. Velocity field

A six element Kenics mixer with open tube entrance and exit sections (Fig. 1) was chosen as a case study. The system geometry and fluid properties are given in Table 1. The inlet velocity adopted in the simulation is $v_x = 0.0012$ m s^{-1}, giving an open tube Reynolds number ($\mathrm{Re} = \rho\langle v_x\rangle D/\mu$) of 0.15. A flat velocity profile is used as the inlet boundary condition at the entrance to the mixer geometry. This boundary condition creates developing flows, which are confined to a region approximately 3.0 cm in length at the start to the open tube entrance section. Downstream of this entrance length, a well developed parabolic flow profile is obtained.

Table 1
Mixer geometry and fluid properties

Mixer	
Diameter (D)	5.08
Plate thickness	0.3175 cm
Entrace length	10.16 cm
Exit length	10.16 cm
Fluid	
Density (ρ)	1.20 g/cc
Viscosity (μ)	500 cp

A commercially available computational fluid dynamics (CFD) software package (FLUENT/UNS) was used to obtain the velocity field for the static mixer. A full discussion of the grid generation, grid validation, and solution procedure using this software has been presented elsewhere [9]. Previous computational investigations of mixing performance in the Kenics mixer by other authors have utilized idealized velocity fields that ignored developing flows at the transitions between mixer elements in order to obtain an analytical solution for the de-coupled axial, radial, and rotational flows [10–13]. However, previous work suggests that the flow areas neglected in idealized analytic solutions (developing flows at element transitions) are the areas that provide the greatest contribution to mixer performance [9]. In contrast to approximate analytic solutions, the use of CFD provides a high quality numerical solution for the velocity field, including developing flows, without the need for additional simplifying assumptions (although such improvements require significantly more intensive computations). This numerical solution then serves as a starting point for further characterization of the mixer performance through the use of Lagrangian particle tracking techniques, which are described next.

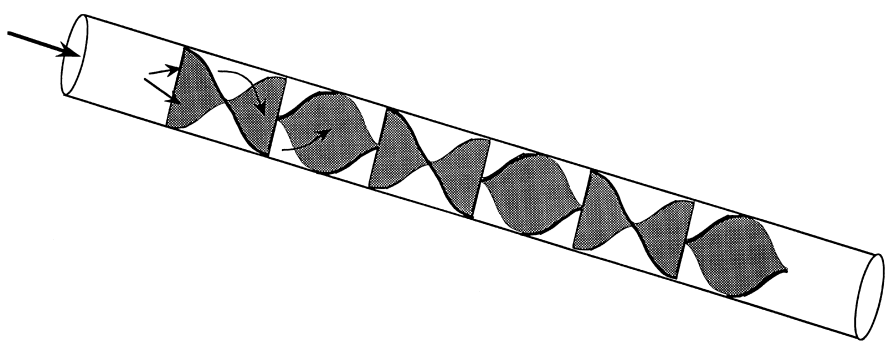

Fig. 1. A six-element Kenics static mixer.

2.2. Particle tracking

Computer software was developed to track fluid particles as they move through the flow field. The movement of the particles is determined by integrating the vector equation of motion

$$\frac{d\boldsymbol{x}}{dt} = \boldsymbol{v}(\boldsymbol{x}) \quad (1)$$

for each particle. A fourth order Runge–Kutta integration scheme with adaptive step-size control [14] was adopted for integration of the equation of motion owing to its high accuracy and straightforward implementation. The three-dimensional discretized velocity field generated by the CFD calculations is used as input to this tracking program.

The flow solution is obtained by dividing the flow domain into ten-node tetrahedra. At each node, the position (x, y, z) and the velocity components (v_x, v_y, v_z) are known. Since the velocity values are only known at discrete node positions, the particle tracking software incorporates a scheme to interpolate the known velocities from the tetrahedral nodes to obtain the velocities at an arbitrary point within a given tetrahedron [9]. The software also provides an efficient means of determining which tetrahedra the particle visits as it moves through the flow. During the tracking computations, a small number of particles ($\sim$5%) become trapped in flow regions near walls of the mixer owing to discretization error. In principle, this problem could be minimized by increasing the refinement of the flow solution. Unfortunately, even the present level of discretization severely strains computational resources, making additional grid refinement impractical at the present time. A different approach is used to solve this problem: whenever a particle touches a wall, it is displaced a very small distance $(10^{-5}R)$ perpendicular to the wall.

For the low Reynolds numbers considered here, the velocity field shows a periodicity matching that of the Kenics mixer geometry [9]. The particle tracking software takes advantage of this periodicity to extend the simulation results for a six-element mixer to devices of greater length. The six-element base case is divided into an entrance section (inlet tube and first two Kenics elements), exit section (outlet tube and Kenics elements 5 and 6), and central periodic section (Kenics elements 3 and 4). Within the particle tracking software, the central section is repeated as a spatially periodic unit to extend the tracking to a mixer of any length. Using this software, particle tracking computations were performed to simulate the flow and mixing of fluids within the Kenics mixer. Tracking 20 000 particles through a 44 element mixer required 110 Mb of RAM and a total of 288 h of CPU time on a dual processor Sun hyperSPARC 20/712 workstation. The results of the particle tracking simulations are described in the next section.

3. Results

3.1. Residence time distribution (RTD)

The RTD for fluids in a Kenics mixer was calculated by tracking $\sim$20 000 uniformly spaced particles initially placed in the open tube region 0.1 cm before the leading edge of the first Kenics element, covering the entire mixer cross-section (the initial axial position of the particles is in the well developed flow region, after the entrance effects due to the inlet boundary condition have disappeared). Particle trajectories were tracked through the flow via integration of Eq. (1), and particle positions and residence times τ were recorded each time a particle crossed a periodic plane within the mixer (i.e. after the 2nd element, 4th element, 6th element, etc.). This information allowed the calculation of a residence time distribution at the specified plane. Given the values of τ for all of the points which have passed the cross-sectional plane, the fraction of the total flow volume that had residence time values between τ and $\tau + d\tau$ was computed as the total number of particles that had residence time values between τ and $\tau + d\tau$, with each particle weighted by the inlet flow that it represents. The proper weighting for each particle was computed as the cross-sectional area represented by the particle multiplied by the inlet axial velocity of the particle, $v_{x,\text{in}}$. The cumulative residence time distribution $F(\tau)$ for a given value of τ was estimated as

$$F(\tau) = \frac{\sum_{t=0}^{\tau} v_{x,\text{in}} dA}{Q_{\text{in}}} \quad (2)$$

where Q_{in} is the total inlet volumetric flow rate. Finally, the actual residence time τ was normalized by the residence time of a particle traveling at the average volumetric flow rate to obtain the normalized residence time θ. The residence time distributions for mixers containing 4, 8, 16 and 32 elements are shown in Fig. 2(a), along with the RTDs which correspond to Poiseuille flow in an open tube (parabolic velocity profile) and to plug flow. The RTDs for the Kenics mixer have a sigmoid shape, which asymptotically approaches the plug flow RTD as the number of mixer elements is increased.

Experimental residence time distribution data for the Kenics mixer have been presented in the literature by Tung [15], Pustelnik and Petera [16] and Pustelnik [17] and can be compared to the simulation results. However, examination of the experimental technique and analysis used in these previous studies reveals that the reported results do not represent the true residence time distribution, but an alternate distribution which is weighted based on the cross-sectional area of the inlet fluid rather than volumetric flow rate. In order to facilitate comparison of the simulation results with the literature data, an area-weighted distribution $F(\theta)$ was computed from the particle tracking simulation results for the Kenics mixer and is shown along with the literature data in Fig. 2(b–d). Qualitatively, the experimental and simulated RTDs both

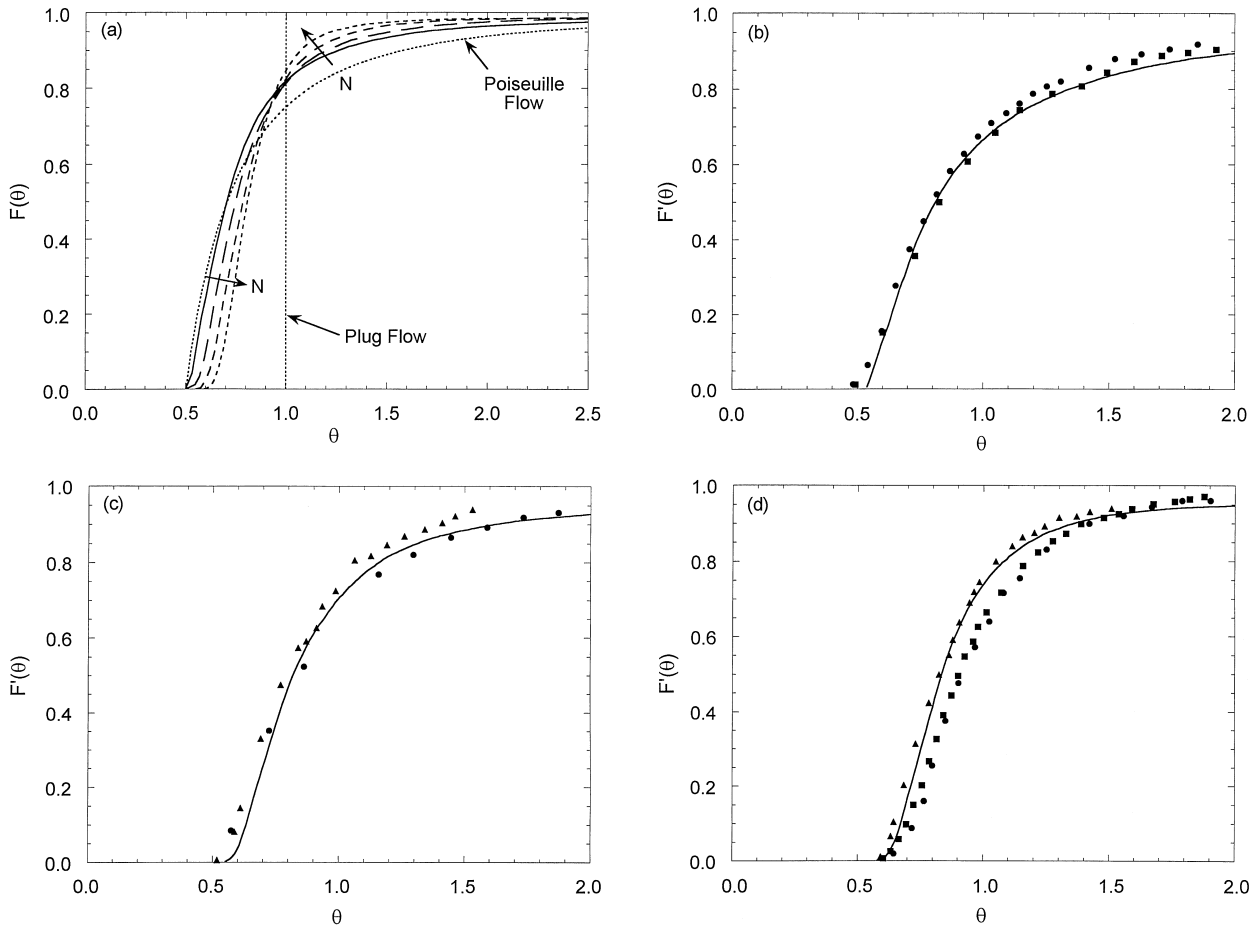

Fig. 2. (a) Residence time distribution vs. the number of mixer elements from the simulation results. The arrows denote the direction that the curves shift with an increasing number of elements (——— $N=4$; —— — $N=8$; — — — $N=16$; - - - $N=32$). (b–d) Simulated area-weighted residence time distributions vs. experimental data from the literature (——— simulation results; ▲ data from Tung [15]; ■ data from Pustelnik and Petera [16]; ● data from Pustelnik [17]). Figures correspond to (b) 4 mixer elements, (c) 8 mixer elements, and (d) 16 mixer elements.

exhibit sigmoid shaped curves which approach the plug flow profile as the number of mixing elements is increased. The agreement is very good and well within experimental error, particularly in the region $\theta \leq 1.5$. While the agreement is slightly less satisfying in the tail region of the RTD ($\theta > 1.5$), this region is subject to the greatest experimental difficulties because, for a pulse injection of tracer, resolution of the region where $F'(\theta) > 0.9$ requires detection of the lowest concentrations of tracer.

3.2. Mixing simulation

Mixing of equal portions of two similar fluids was simulated also for ~20 000 particles placed uniformly to cover the entrance to the mixer (Fig. 3(a)). The particles were tracked through the flow and their cross-sectional positions recorded when the particles crossed the planes after the 2nd Kenics element, 4th element, 6th element, etc. The structures obtained at each cross-section are shown in Fig. 3(b–f). These cross-sections represent the structures which would be present at the corresponding planes for a mixer in steady-state operation with a continuous feed having the composition shown in Fig. 3(a). Fig. 3(b–f) shows the reduction in thickness of the striations as mixing takes place. After 10 elements, individual striations are no longer visible with the resolution provided by this number of particles.

Several authors [18–20] have reported the correlation $S=2^n$ for the number of striations, where S is the number of striations and n is the number of Kenics elements. An examination of Fig. 3(b) and (c) reveals that this pattern of striation evolution is confirmed in the simulation results for the initial mixer segments. $S=2^2=4$ striations are present after the 2nd Kenics element (Fig. 3(b)), and $S=2^4=16$ striations can be observed after the 4th element (Fig. 3(c)). However, as mixing progresses, it quickly becomes impossible to identify and count individual striations.

The simulation results from Fig. 3 are qualitatively identical to experimental results that have been reported for mixing of two initially segregated fluids. Cross-sectional slices from such mixing experiments have been presented in well known studies by Grace [21] and Middleman [19]. Exact quantitative comparison between the experimental results and the simulation is difficult, owing to uncertainties in the exact locations of the slices from the experimental work. However,

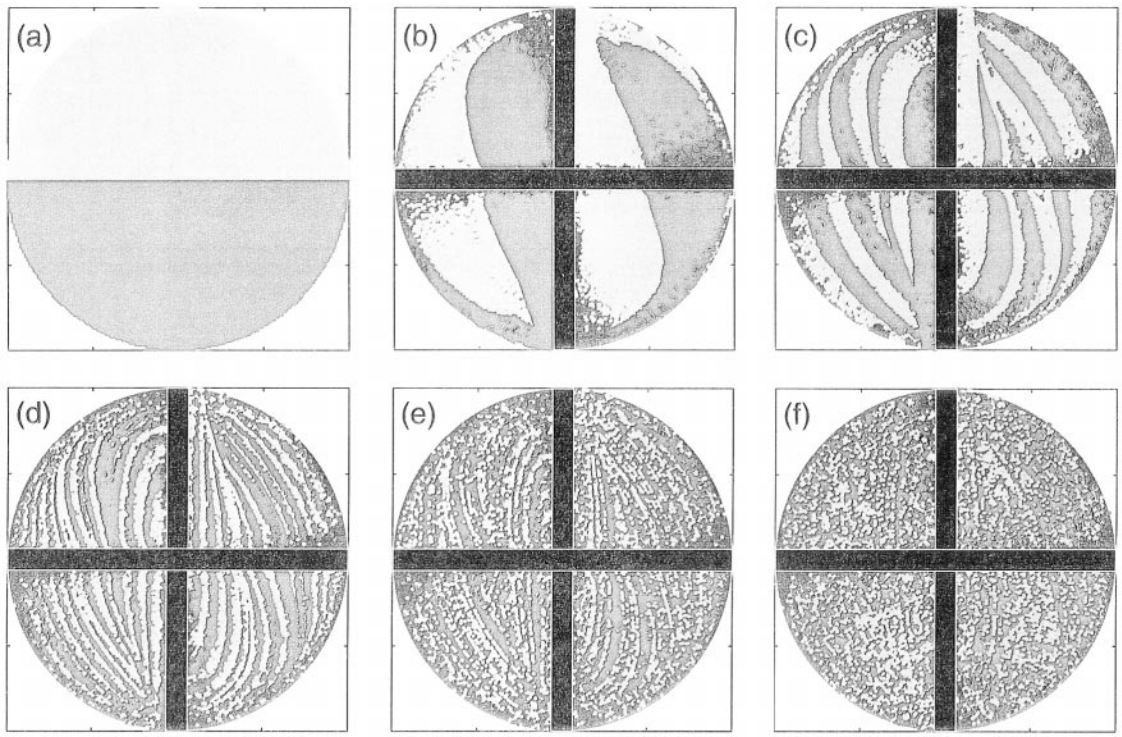

Fig. 3. Cross-sectional profiles for equal volume mixing of two initially segregated components. Cross-section locations: (a) inlet; (b) after 2 elements; (c) after 4 elements; (d) after 6 elements; (e) after 8 elements; (f) after 10 elements.

a qualitative comparison reveals similar evolution of striation patterns as the fluid moves down the mixer.

A second type of mixing simulation was performed in order to study the behavior of a small amount of tracer injected into the flow. For this simulation, ~20 000 uniformly spaced particles were placed in a small circle with a radius equal to 1% of the mixer radius at $y=0.5$ cm, $z=0.5$ cm, 0.1 cm upstream of the leading edge of the first mixer element (Fig. 4(a)). Again, the particles were tracked through the flow and their cross-sectional positions were recorded when the particles crossed the plane after the 2nd Kenics element, and every spatial period thereafter. The structures obtained at each cross-section are shown in Fig. 4(b–l). The evolution of the structures illustrates the mechanisms that contribute to mixing in the Kenics mixer. The initial circle of points is stretched into a ribbon, which is elongated, re-oriented, and folded by the flow within individual elements. The ribbon of tracer is also cut by the leading edges of sequential mixer elements. The tracer initially occupies a small fraction of the total flow, but is redistributed by the mixing action to cover nearly all of the flow domain after 16 elements.

The results in Fig. 4 are presented for a single tracer injection location. Variation in the injection point will somewhat affect the partially mixed structures that are produced in the first few mixing elements (Fig. 4(a–f)). However, owing to the chaotic nature of the Kenics flow, the structure obtained after many flow periods is robust and insensitive to the initial injection location. The mixed structures present after many elements (Fig. 4(h–l)) reflect the underlying structure of the periodic manifolds present in the flow and do not depend on the tracer introduction point [4] (the manifold structure and its effect on mixing in the system is covered in greater detail in Section 3.4).

3.3. Variation coefficient

While the evolution of patterns of striations provides a useful qualitative understanding of the progress of fluid mixing within the static mixer, a quantitative description of the mixture quality provides a more practical means of evaluating mixer performance. Building on the intensity of segregation concept from Danckwerts [22], mixture quality has often been quantified in terms of a mixing index which describes the degree of homogeneity of the system. The mixture homogeneity is evaluated based on a statistical analysis of samples from the mixture, with the mixing index expressed as a function of the standard deviation (σ) or variance (σ^2) of the mixture samples. The mixture variance is defined as

$$\sigma^2 = \frac{\sum_{i=1}^{n} (C_i - \bar{C})^2}{n-1} \tag{3}$$

where C_i is the concentration of the i^{th} sample, $\bar{C}$ is the mean value of concentration, and n is the number of samples.

Experimental data for mixture quality in the Kenics static mixer has been reported in terms of the variation coefficient $\sigma/\bar{C}$ [23,24], also known as the relative standard deviation (RSD). In order to facilitate a comparison with the available experimental data, the variation coefficient was computed for the cross-sectional profiles generated from mixing simula-

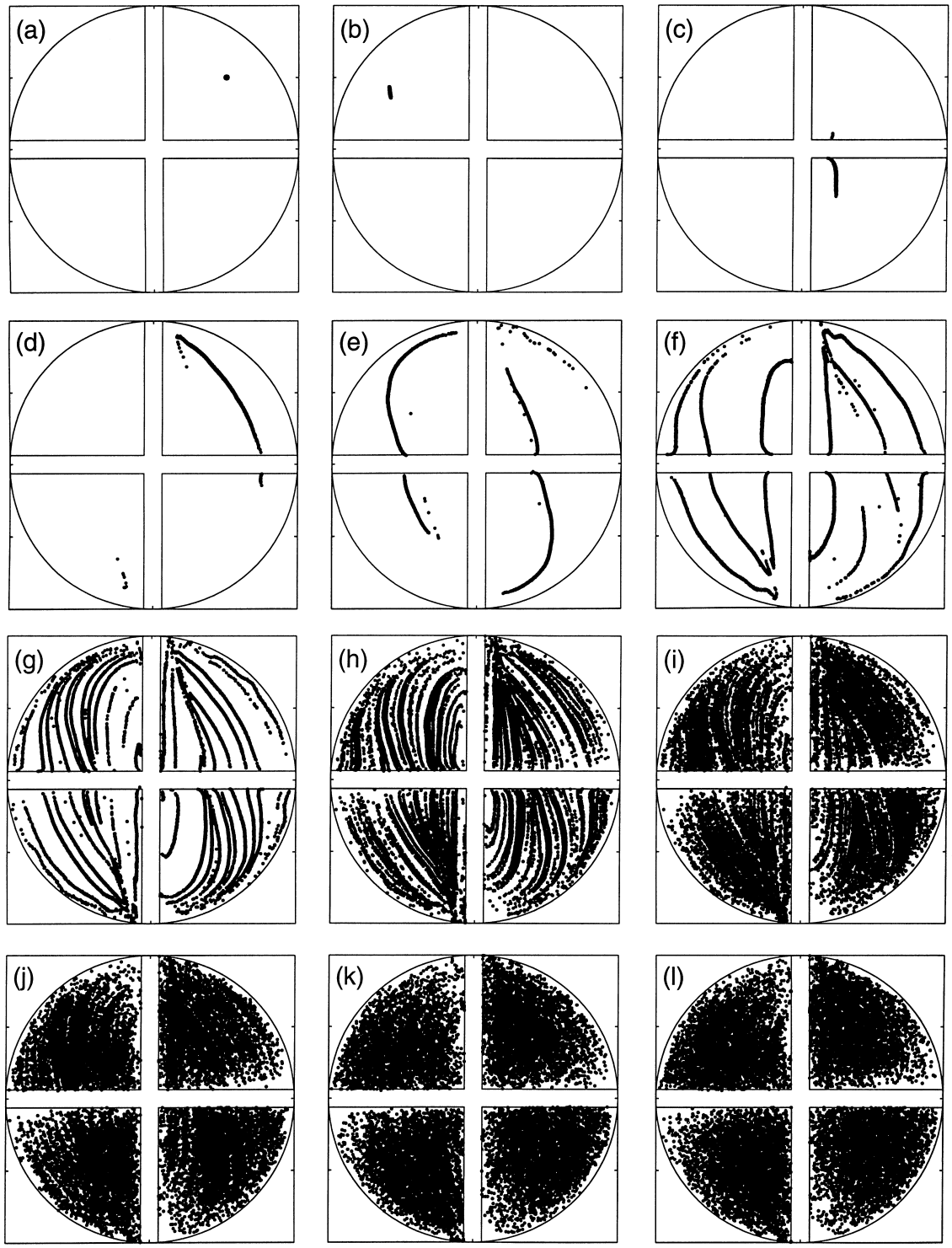

Fig. 4. Cross-sectional profiles for tracer mixing. The initial tracer is injected at the point $y=0.5R$, $z=0.5R$. Cross-section locations: (a) inlet; (b) after 2 elements; (c) after 4 elements; (d) after 6 elements; (e) after 8 elements; (f) after 10 elements; (g) after 12 elements; (h) after 14 elements; (i) after 16 elements; (j) after 18 elements; (k) after 20 elements; (l) after 22 elements.

tions. The data of Allocca [23] and Pahl and Muschelknautz [24] were obtained for $\bar{C}=0.10$ (i.e. a 10% injection of tracer), with tracer apparently injected at the center of the mixer tube. In order to provide a comparison with these experimental data, a 10% tracer mixing simulation was conducted as follows: 20 000 uniformly spaced particles were placed in a circle centered at ($y=0$, $z=0$), 0.1 cm upstream of the leading edge of the first Kenics element, with the circle of particles covering an area representing 10% of the volumetric flow on that cross-section. The particles were tracked through

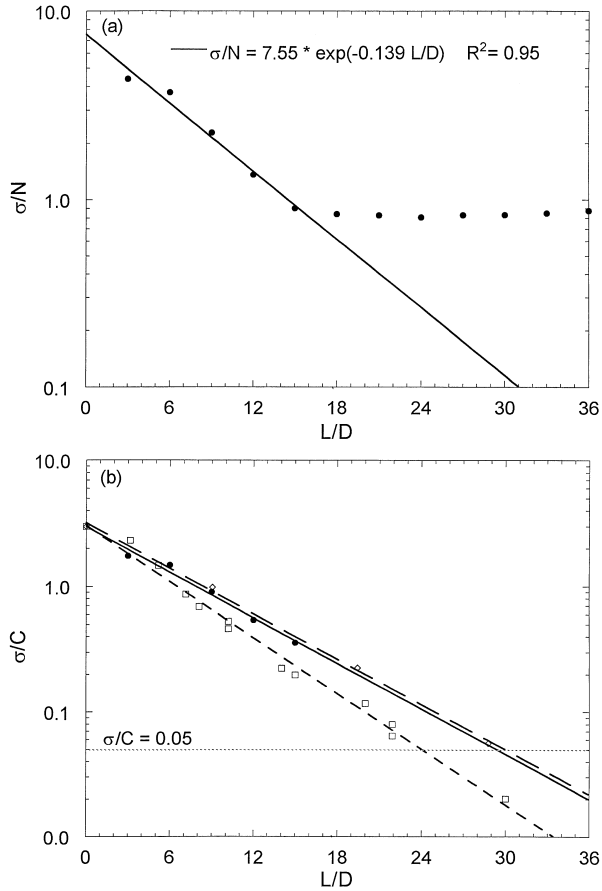

Fig. 5. Variation coefficient vs. normalized mixer length L/D. (a) Simulation results. The number-based variation coefficient σ/N is computed instead of the concentration based variation coefficient σ/C. (b) Normalized simulation results vs. experimental data from the literature (——●—— simulation results; — ◇ — data from Allocca [23]; — □ — data from Pahl and Muschelknautz [24]).

the flow and their positions recorded where the particles cross the plane after the 2nd Kenics element, and every spatial period thereafter.

The variation coefficient on a given mixer cross-section is calculated as follows. A square grid of 64×64 cells is laid out to cover the mixer cross-section. Cells that fall entirely within the flow domain are retained as 'live' cells for calculation purposes, while cells which fall partially or completely outside of the flow domain are considered 'dead'. A total of $n = 2600$ live cells are obtained. Subsequently, the number of particles in each live cell (N_i) and the total number of particles which fall within the live cells (N_{tot}) are computed based on the position of each particle on the mixer cross-section. The average number of particles per cell is then computed as $\bar{N} = N_{tot}/n$. The variance σ_N^2 is then computed via Eq. (3) with N_i in place of C_i and $\bar{N}$ in place of $\bar{C}$ to obtain the number-based variation coefficient $\sqrt{\sigma_N^2}/\bar{N}$.

The results for the number-based variation coefficient vs. normalized mixer length (L/D) are shown in Fig. 5(a). The calculated variation coefficient decreases monotonically from the inlet of the mixer up to $L/D = 15$ (10 mixer elements). After this point, the variation coefficient levels out, indicating that the characteristic length for the mixture has fallen below the scale of the grid size used for calculation, and further homogenization of the mixture cannot be determined at this level of resolution. The scale for the grid is limited by several factors. The variation coefficient is calculated based on a finite number of discrete tracked points, and a minimum number of points per cell must be maintained to minimize statistical uncertainty. Hence, the number of grid cells cannot be increased indefinitely. For the case described with $N_{tot} = 20\,000$ and $n = 2600$, $\bar{N} = 7$–8 points/cell. Based on a striation evolution that follows $S = 2^n$, the striation thickness correspondingly decreases proportional to 2^{-n}, and each periodic unit (two mixer elements) results in an approximate four-fold reduction in the mixture length scale. Therefore, in order to resolve the variation coefficient for one additional period, a sixteen-fold increase in the number of grid cells would be required, with a corresponding sixteen-fold increase in the number of tracked particles in order to maintain an equivalent value for $\bar{N}$. Such an increase in the number of particles would require an extremely long computation time (on the order of 1000 h CPU time on a Sun SPARC 20/712) only to increase the number of elements from 10 to 12. This marginal increase does not justify the increase in computational time. Therefore, the variation coefficient data for the first 10 mixer elements are used for further calculations.

As shown in Fig. 5(a), the exponential reduction in variation coefficient over the first 10 mixer elements can be correlated by an equation of the form

$$\frac{\sigma}{\bar{N}} = A \exp\left(-B\frac{L}{D}\right) \tag{4}$$

which is frequently used to describe data of this type [25]. The coefficients $A = 7.55$ and $B = 0.139$ are regressed from the simulation results. The coefficient B represents the rate of decrease in the variation coefficient per unit mixer length, while the coefficient A is the variation coefficient of the unmixed inlet stream. For a completely segregated inlet stream with $\bar{C} = 0.1$, the concentration-based variation coefficient is

$$\frac{\sigma_0}{\bar{C}} = \sqrt{\left(\frac{1}{\bar{C}} - 1\right)} = 3.0 \tag{5}$$

To provide a direct comparison with concentration-based experimental data, the number-based variation coefficient (Eq. (4)) was rescaled by $(\sigma_0/\bar{C})/A = 0.40$, resulting in a vertical shift of the data while maintaining the slope unchanged.

Fig. 5(b) shows the rescaled simulation results for the first 10 mixer elements plotted along with the experimental data reported by Allocca [23] and by Pahl and Muschelknautz [24]. For the two sets of experimental data, the data of Allocca [23] are consistently larger, suggesting that the effective sample size was smaller than that used by Pahl and Muschelknautz [24]. Despite the differences, both sets of data have similar slopes. Both studies also produce similar

predictions for the value of L/D required to achieve $\sigma/\bar{C}=0.05$, which is often (arbitrarily) used as criterion for a well mixed system. In particular, the two sets of data for the Kenics mixer are consistent with one another when viewed in comparison to the other types of mixers which were also examined in the original papers [25]. The current simulation results match the results from the previous studies within the experimental deviations.

The agreement between simulation results and experimental data for residence time distributions, striation development, and variation coefficient confirm that the simulation provides a reasonably accurate description of the Kenics mixer. These measures of mixing performance provide an average description of mixer behavior but do not allow a detailed description of the mixing process within the flow. Computation of the stretching field in mixing flows can be used to provide a more complete description of the dynamics or spatial structure of the mixing process in specific regions of the flow. The application of this Lagrangian technique to the Kenics mixer is described next.

3.4. Stretching histories

Several recent studies have shown that the evolution of partially mixed structures in a flow system can be determined by computing the deformation (stretching) and trajectories of a set of material elements placed within the flow [4–6,26–28]. The amount of intermaterial surface generated in a region of the flow is directly proportional to the amount of stretching experienced by material elements in that region. The rate of stretching determines the rate of the micromixing process both by increasing the intermaterial area over which inter-diffusion of components can occur, and also by decreasing the required diffusional distance. The positions of points experiencing high and low stretching correspond to regions of good and poor micromixing, respectively, and the distribution of stretching magnitudes provides a means for characterizing the distribution of mixing intensities within the flow (for a more detailed discussion, see Liu et al. [29]).

Previous studies have investigated the evolution of stretching histories for points in two-dimensional, time-periodic flow systems which exhibit chaotic behavior [3,4,29,30]. The current investigation applies techniques drawn from these previous studies in order to characterize stretching in the Kenics mixer. To the best of our knowledge, *this study represents the first application of such techniques to a complex, three-dimensional, industrial mixing system.*

Stretching histories for material elements are computed as follows. In addition to tracking the position of tracer particles placed into the simulated velocity field, the tracking software described in Section 2.2 is used to compute the stretching of a fluid element $\boldsymbol{l}$ associated with each tracer particle. The evolution of the vector $\boldsymbol{l}$ is tracked by integrating Eq. (1) (element position) along with:

$$\frac{\mathrm{d}(\boldsymbol{l})}{\mathrm{d}t}=(\nabla \boldsymbol{v})^{\mathrm{T}}\cdot\boldsymbol{l},\ \boldsymbol{l}_{t=0}=\boldsymbol{l}_0 \tag{6}$$

The total accumulated stretching λ experienced by the element after some time is defined as

$$\lambda=\frac{|\boldsymbol{l}|}{|\boldsymbol{l}_0|} \tag{7}$$

For the stretching calculations, ~20 000 particles were placed to cover uniformly the entrance to the mixer (the same initial conditions as shown in Fig. 3(a)). Each particle was assigned an initial stretch vector $\boldsymbol{l}_0=[1,0,0]$. The particle position and accumulated stretching were tracked through the flow via integration of Eqs. (1) and (6). At each periodic plane, the position and components of the stretch vector $\boldsymbol{l}$ were recorded. A total of ~456 h CPU time were required to compute λ for 20 000 particles through a 44 element mixer. The CPU time required for stretch tracking is significantly greater than that for position tracking alone because twice as much information is being computed for each point at each time step (three components of the position vector plus three components of the stretch vector).

At each periodic plane, the geometric mean of the stretching values for all N points is computed:

$$\langle\lambda_{\mathrm{g}}\rangle=\left(\prod_{i=1}^{N}\lambda_i\right)^{\frac{1}{N}} \tag{8}$$

The logarithm (base 10) of $\langle\lambda_{\mathrm{g}}\rangle$ is plotted in Fig. 6 vs. the number of mixer elements, where $\Lambda_n=\log_{10}\langle\lambda_{\mathrm{g}}\rangle$ after the nth spatial period, or after $2n$ mixer elements. During the first two mixer elements, the initial orientations of the stretch vectors are realigned to correspond to the principal stretching directions of the flow. After this realignment, the initial vector orientations are no longer important. The mean stretch grows at a steady exponential rate vs. the number of mixer elements. This exponential growth of stretching, which corresponds to an exponential generation of intermaterial area as fluid flows through the mixer, is one of the defining features of a chaotic

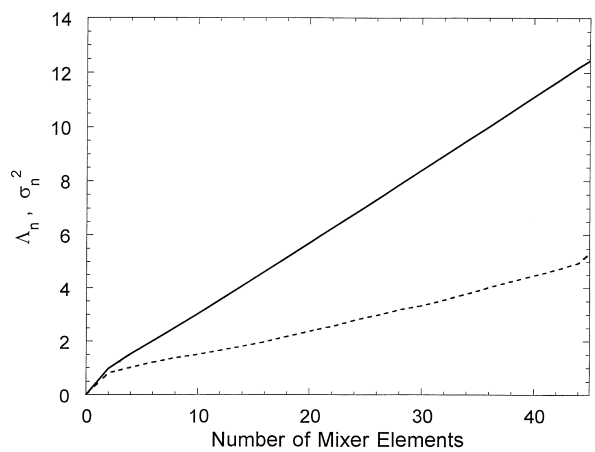

Fig. 6. Mean ($\Lambda_n=\log_{10}\langle\lambda_{\mathrm{g}}\rangle$) and variance ($\sigma_n^2$) of the logarithm of stretching vs. the number of mixer elements (——— Λ_n; —— —— σ_n^2).

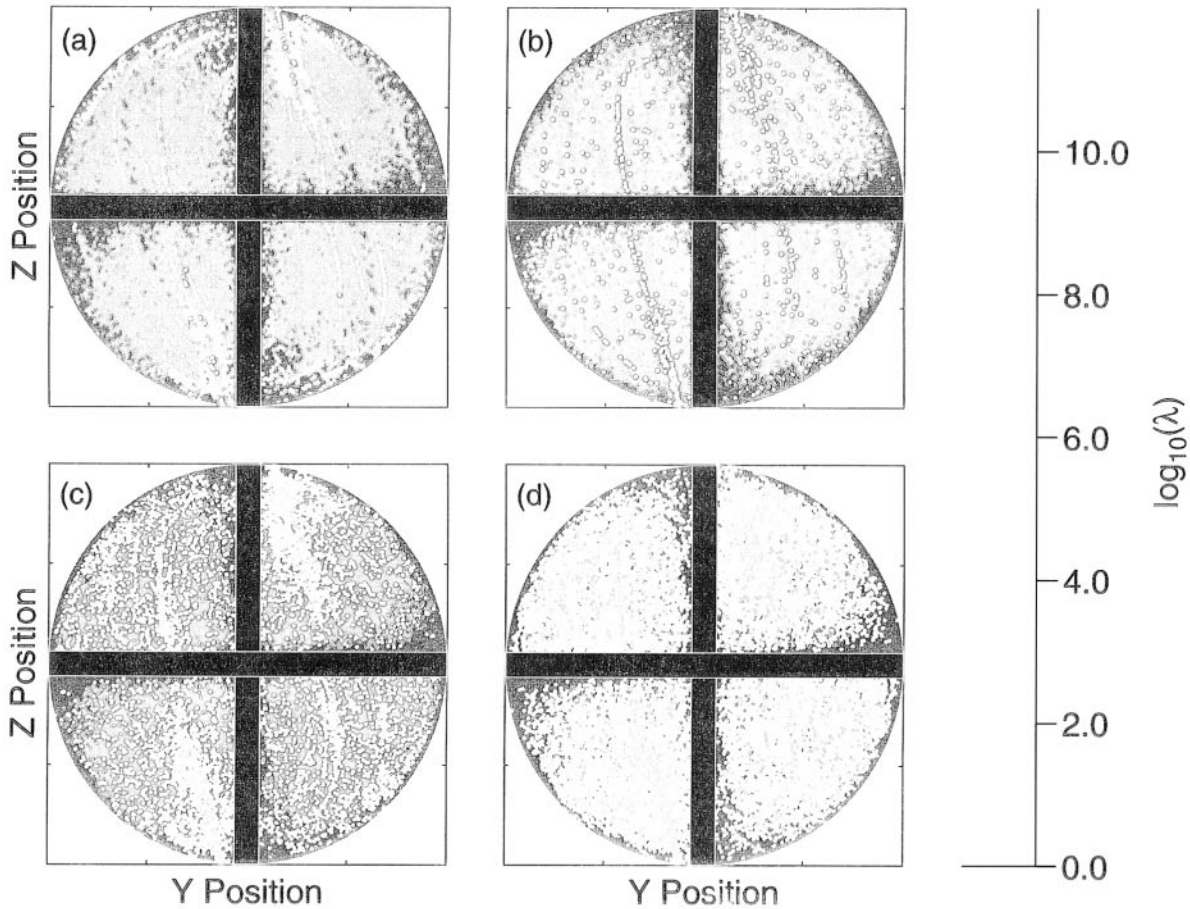

Fig. 7. Cross-sectional profiles of the logarithm of stretching, $\log_{10}\lambda$. Cross-sections are located after (a) 4 elements, (b) 12 elements, (c) 20 elements, (d) 28 elements. The magnitude of $\log_{10}\lambda$ is represented by the color scale at right.

flow. The exponential stretching rate can be described in terms of the specific stretching per period α, defined as

$$\alpha = \lim_{n\to\infty}\left[\frac{1}{N}\ln\langle\lambda_g\rangle\right] \quad (9)$$

The specific stretching for a spatially periodic flow is the direct analog of the Lyapunov exponent in a time periodic system. For the flow system under investigation, $\alpha = 1.233$. The variance of the logarithm of the stretching, σ_n^2, is also plotted in Fig. 6 and increases linearly with the number of mixer elements. The significance of this variance will be described later.

The overall structure of the stretching field can also be examined. A plot of the spatial distribution of stretching at several mixer cross-sections is shown in Fig. 7. The positions of the dots correspond to the cross-sectional position where the tracked tracers cross the plane. The color of the dots represents the logarithm of the stretching magnitude, $\log_{10}(\lambda)$, where λ is calculated via Eq. (9). The color scheme is shown at the right of the figure: dark blue and light blue correspond to low stretching, green and yellow to intermediate values, and magenta and red to the highest stretching. A general increase in stretching values with progress through the mixer is observed, consistent with the exponential growth in mean stretching shown in Fig. 6. On each cross-section, a distribution of stretching values is observed, with some regions exhibiting stretching significantly higher than the mean (yellow areas in Fig. 7(a)) while other regions exhibit stretching which is below the mean (green areas in Fig. 7(d)). Owing to the exponential increase of stretching, the distribution of λ values is best described using the probability density function of the logarithm of stretching values $H_n(\log_{10}\lambda) = (1/N)\mathrm{d}N(\log_{10}\lambda)/\mathrm{d}\log_{10}\lambda$, which is computed for each periodic plane by counting the number of points $\mathrm{d}N(\log_{10}\lambda)$ that have stretching values between $\log_{10}\lambda$ and $\log_{10}\lambda + \mathrm{d}(\log_{10}\lambda)$. Conceptually, $H_n(\log_{10}\lambda)$ can be interpreted as a spectrum of intensities in the micromixing process. Fig. 8(a) shows a plot of $H_n(\log_{10}\lambda)$ on several selected mixer cross-sections (periodic planes after 4, 12, 20, 28, 36, and 44 mixer elements). The $H_n(\log_{10}\lambda)$ vs. $\log_{10}\lambda$ plots obtained for the Kenics mixer appear qualitatively similar to curves which have been reported for chaotic regions of two-dimensional, time-periodic flows such as the cavity flow [29,30] and the egg-beater flow [5]. As the number of mixer elements increases, stretching accumulates and the curves shift toward higher values of $\log_{10}\lambda$. After the first few elements, the central portion of the curve begins to approach a bell-shaped, Gaussian profile which describes the spectrum

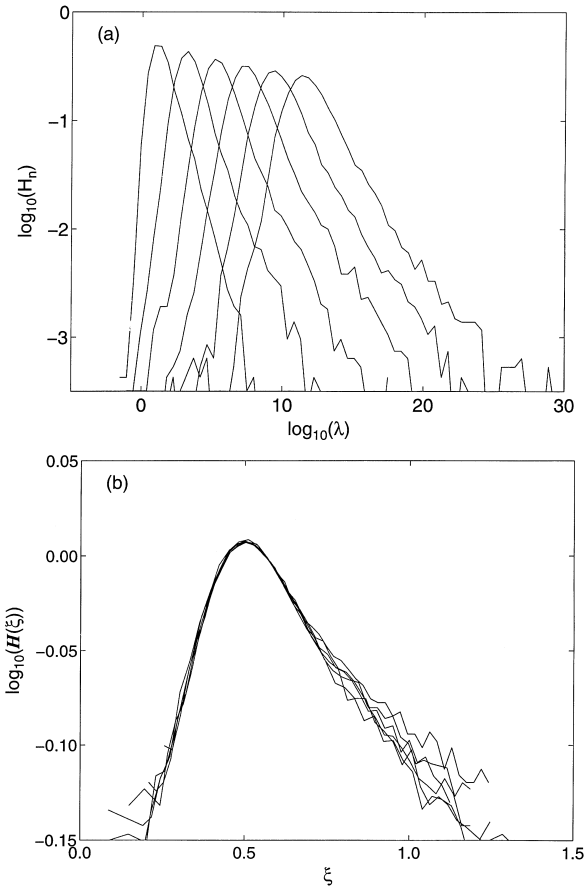

Fig. 8. (a) Probability density function of the logarithm of stretching values, $H_n(\log_{10}\lambda)$, plotted for 4, 12, 20, 28, 36, and 44 elements. The curves shift from left to right as the number of mixer elements is increased. (b) $\boldsymbol{H}(\xi)$ as defined by Eq. (12), plotted for periods $n=16$, 17, 18, 19, 20, and 21.

of stretching intensities for the bulk of the flow. Such distributions are typical of globally chaotic flows. The curves also exhibit long tails on the high stretching side, indicating that a subset of points experiences very high stretching (which is also evident from the cross-sections in Fig. 7). The absence of extended tails or a significant 'bump' on the low-stretching side of the curves indicates that there are no large islands of regular, non-chaotic behavior present in the flow.

Another tool that has been applied to characterize the stretching distributions in two-dimensional chaotic flows is the evolution of an asymptotic scaling relation for $H_n(\log_{10}\lambda)$. As discussed by Muzzio et al. [4], the stretching accumulated by an individual vector i from the beginning of the first period to the end of the nth period, $\lambda_{0,n}(i)$, can be expressed as the product of the stretchings $\lambda_{j-1,j}(i)$ accumulated during each period j. The central limit theorem predicts that when the statistics of the stretching multipliers are independent of the period, $H_n(\log_{10}\lambda)$ should asymptotically evolve into a Gaussian distribution around its mode,

$$H_n(\log\lambda_{0,n}) = [2\pi\sigma_n^2]^{-1/2}\exp\left[-\frac{(\log\lambda_{0,n}-\Lambda_n)^2}{(2\sigma_n^2)}\right] \quad (10)$$

where Λ_n and σ_n^2 are the mean and variance of the variable $\log\lambda_{0,n}$. The central limit theorem also predicts that for large enough n, Λ_n and σ_n^2 will evolve linearly with n as

$$\Lambda_n \approx n\Lambda \text{ and } \sigma_n^2 \approx n\sigma^2 \quad (11)$$

where Λ and σ^2 are the mean and variance of the logarithms of the multipliers for a single period. Fig. 6 illustrates that linear growth of the mean and variance of $\log\lambda_{0,n}$ with the number of mixer elements is observed for the Kenics mixer, confirming the predictions of Eq. (11) for this flow system.

Using Eqs. 10 and 11, Liu et al. [30] proposed an asymptotic scaling relationship for $H_n(\log_{10}\lambda_{0,n})$ in terms of a function $\boldsymbol{H}(\xi)$,

$$\boldsymbol{H}(\xi) = \exp\left[\frac{-(\xi-\Lambda)^2}{(2\sigma^2)}\right]$$
$$= \{[2\pi\sigma_n^2]^{1/2}H_n(\log\lambda_{0,n})\}^{1/n} \quad (12)$$

which is invariant with the number of flow periods, where the new variable $\xi=(1/n)\log\lambda_{0,n}$ was defined as the short-time Lyapunov exponent. Eq. (12) implies that curves for $H_n(\log_{10}\lambda_{0,n})$ corresponding to different periods should collapse to an invariant limit when plotted as $\boldsymbol{H}(\xi)$. Again drawing the analogy with time-periodicity, Eq. (12) was used to rescale the $H_n(\log_{10}\lambda)$ distributions for the Kenics mixer for different numbers of spatial periods, corresponding to different numbers of mixer elements. The results are plotted in Fig. 8(b) for periods 16 through 21. The scaled curves slowly collapse to an invariant solution for most values of ξ ($\xi<0.8$) as the number of periods increases. This represents the majority of particle trajectories in the flow. However, the scaling fails for higher values of ξ, corresponding to the tails of $H_n(\log_{10}\lambda)$ that are created by a small number of particles that are present in high stretching regions in the flow. The breakdown of the scaling relationship for the tail of the distribution indicates that the initial assumption that the multipliers become uncorrelated is not valid for these high stretching regions. Similar results were presented by Liu et al. [30] for the globally chaotic cavity flow, where an invariant scaling solution was obtained for the bulk of the flow, but the scaling broke down for high stretching regions created by manifolds of periodic points and corner singularities.

In order to examine further the regions of highest stretching in the Kenics mixer flow system, the points with the top 5% of λ values are plotted on six cross-sections in Fig. 9. A stable structure exists for the high stretching regions, as revealed by comparing the different cross-sections. In particular, a streak of high stretching begins near the top right corner of the vertical mixer element, from where it extends down and to the right at approximately a 10° angle from the vertical. A second high stretch streak is symmetrically located, beginning near the bottom left corner of the vertical mixer element edge. Previous studies of the two-dimensional flow between eccentric cylinders [3,6] and of the chaotic cavity flow [29,30] have shown that the short-time spatial structure of high stretching regions in the flow is determined by the struc-

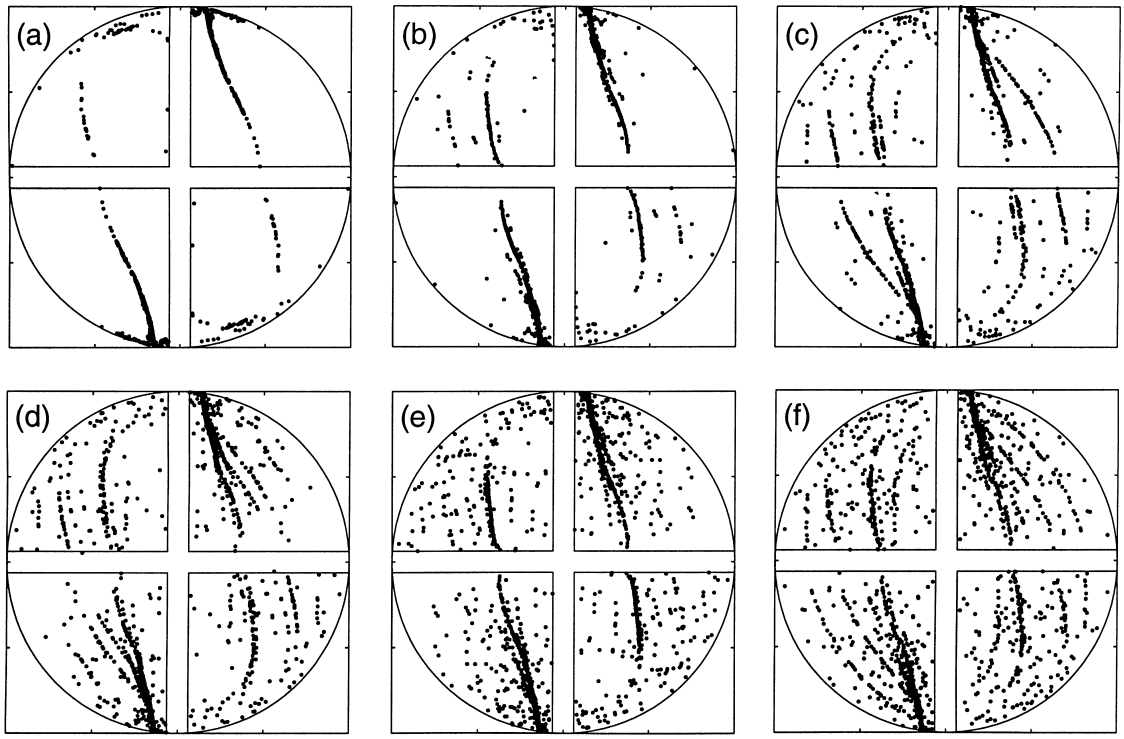

Fig. 9. Cross-sectional profiles showing the points that have the top 5% of values for stretching magnitude λ. Cross-sections are located after (a) 2 elements (1 period), (b) 4 elements (2 periods), (c) 6 elements (3 periods), (d) 8 elements (4 periods), (e) 10 elements (5 periods), (f) 12 elements (6 periods).

ture of the unstable manifolds of hyperbolic periodic points. In order to extend this idea to three-dimensional flows, periodic points and their associated manifolds were located and characterized for the Kenics mixer flow system.

In a two-dimensional, time-periodic flow, a period n point is defined as a fluid point that returns to its initial location after being convected by the flow for n time-periods. Analogously, for the three-dimensional, spatially periodic flow investigated here, the two-dimensional cross-sectional planes after each periodic unit in the Kenics mixer are treated in the same manner as the time-periodic snapshots which are used to construct a two-dimensional Poincaré section. A period n point is defined as a fluid point that returns to its initial cross-sectional position after being convected by the flow for n spatial periods in the axial direction (i.e. after traveling through $2n$ mixer elements). Periodic points are located by covering the flow cross-section with a large number of tracer particles, tracking the tracers through the flow, and identifying those which return to their initial cross-sectional position after a given number of periods. The procedure is refined by placing higher concentrations of tracer particles in the vicinity of suspected periodic points until the location of the periodic point is accurately identified.

Once the periodic points are located, the nature of the points is determined by calculating the deformation tensor $\boldsymbol{F}$ as

$$\frac{\mathrm{d}(\boldsymbol{F})}{\mathrm{d}t} = (\nabla \boldsymbol{v})^{\mathrm{T}} \cdot \boldsymbol{F},\ \boldsymbol{F}_{t=0} = \boldsymbol{I} \qquad (13)$$

where $\boldsymbol{I}$ is the identity tensor. The deformation tensor is computed along the trajectory followed by the periodic point using the same tracking software described above for position and stretch tracking. The nature of the periodic point is determined by the eigenvalues of $\boldsymbol{F}$. For elliptic points, some eigenvalues of $\boldsymbol{F}$ will be complex and the point will be surrounded by an island of regular, non-chaotic flow. For hyperbolic points, all eigenvalues of $\boldsymbol{F}$ are real, and the point will have stable and unstable manifolds which approach and leave the point (respectively) along the eigendirections of the deformation tensor.

Two period-1 hyperbolic points were found in the flow in the Kenics mixer. The points are located symmetrically, at ($y = 0.127R$, $z = 0.984R$) and ($y = -0.127R$, $z = -0.984R$) in the mixer cross-section at the plane between periodic segments. The unstable manifolds for these points were determined by placing 20 000 tracer particles in a small circle (radius $\approx 0.7\%$ of R) around the location of the point at the periodic plane, and tracking the tracers through the flow for several periods. The results of this tracking are shown in Fig. 10, which shows two-dimensional slices of the manifolds at periodic intervals. For a three-dimensional flow system, the manifolds are actually three-dimensional structures; two-dimensional slices of the manifolds are displayed here to facilitate visualization and analysis. The structure of the manifold develops slowly at first (through 4 flow periods) and the tracers reach only a small region of the flow domain. With further progress through the mixer, the tracers spread to cover more and more of the flow cross-section. The complete man-

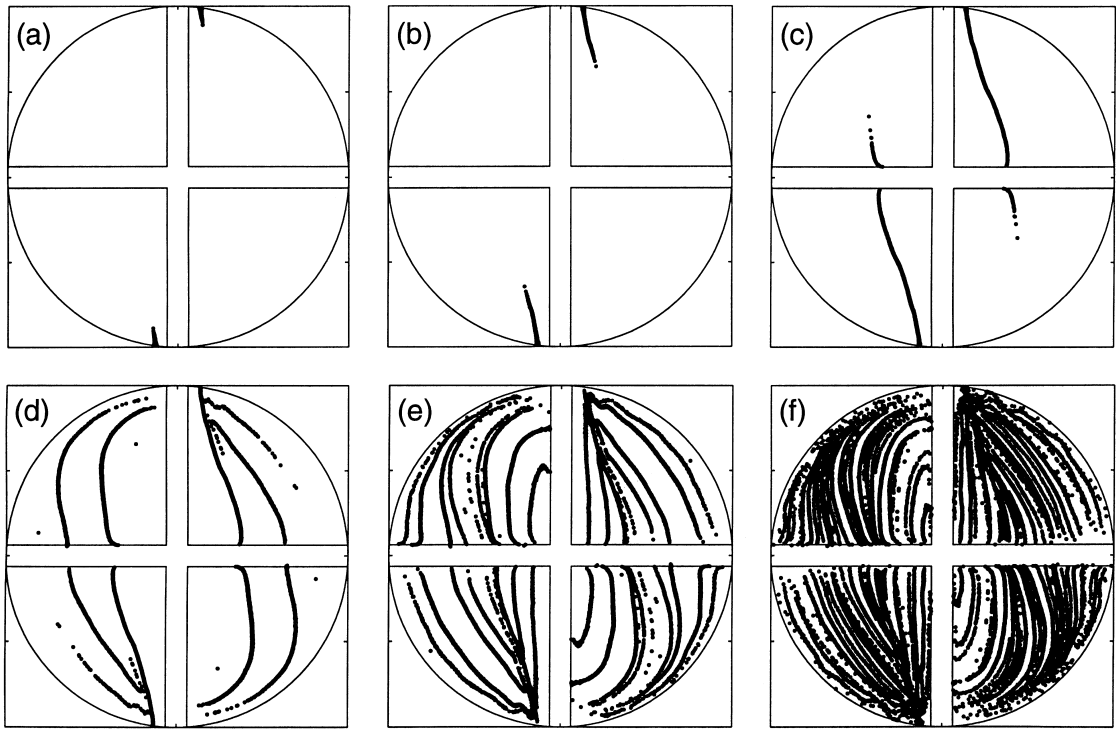

Fig. 10. Cross-sectional profiles showing the manifolds of the two period-1 hyperbolic points that were found in the flow. Cross-sections are located after (a) 2 elements (1 period), (b) 4 elements (2 periods), (c) 6 elements (3 periods), (d) 8 elements (4 periods), (e) 10 elements (5 periods), (f) 12 elements (6 periods).

ifold for the periodic point is an invariant structure (i.e. the structure of the manifold is the same when examined at periodic intervals) and has infinite length. After a sufficient number of periods, manifolds that start inside the chaotic region of the flow will asymptotically approach all points within the chaotic region. However, for mixing processes in actual practice, the number of spatial periods is limited and the manifold effects of interest are those that occur for a small number of periods. Particles initially close to a periodic point travel along the unstable manifold and experience high stretching, but only reach a limited region of the overall flow, resulting in segregated regions of high stretch.

Comparison of the manifolds from Fig. 10(c) and (d) with the high stretching regions from Fig. 9 reveals a good qualitative agreement between the structures. The dominant feature of the low-period manifold is a streak which emanates from the period-1 point in quadrant 1 and stretches down and to the right across the flow cross-section (Fig. 10(a–c)), with a symmetric streak for the quadrant 3 period-1 point. This corresponds exactly to the most densely populated high stretching regions in Fig. 9. For a higher number of periods, the manifold structure develops branches that fan off from the initial streak (Fig. 10(d)). This structure is also evident in the high stretching plots (most notably in Fig. 9(b)), although more faintly than the dominant streak corresponding to the lower-period structure of the manifold.

4. Conclusions

Mixing in a Kenics static mixer was simulated by tracking the motion of a large number of fluid tracer particles via integration of the equation of motion for each particle. The agreement of the simulation results with experimental data from the literature for residence time distributions, striation evolution, and mixing index verifies that the simulation technique accurately represents the physical system. The match between simulation and existing experimental results indicates that the simulation technique can be used as a tool to make a preliminary evaluation of mixing performance for a given mixer geometry.

The stretching histories of fluid tracer particles were also tracked for tracer elements convected by the flow. This technique has been used previously to evaluate mixing and chaotic behavior in two-dimensional, time-periodic flow systems. The current results extend the use of this technique for the first time to the direct evaluation of an actual three-dimensional industrial mixing device. Analysis of fluid filament stretching indicates that the average stretch grows exponentially with the number of flow periods, which is a signature of chaotic flows. Computation of the probability density function of the logarithm of stretching values, $H_n(\log_{10}\lambda)$, reveals a Gaussian distribution over the central spectrum of stretching intensities. Particularly, no deviations

from the Gaussian profile are found at low stretching intensities, suggesting that the flow is globally chaotic. A significant tail of high stretching intensities is also found, however, where the spatial locations of points with the highest stretching values correspond to the manifolds of two period-1 hyperbolic points which are present in the flow. A scaling formalism for $H_n(\log_{10}\lambda)$ based on the central-limit theorem collapses the stretching distributions to an invariant limit over the majority of $\log_{10}\lambda$ values. However, the scaling fails for the high stretch tails, indicating that persistent correlations for the stretching multipliers exist in the high stretch regions.

The results obtained for the Kenics mixer demonstrate that dynamical systems analysis tools can be applied for the analysis of mixing in 'real-world' industrial systems. Coupled with the use of CFD to compute velocity fields for complex geometries, particle tracking and stretch tracking provide a practical means for quantitative analysis of mixing performance. Computational tools such as these provide the means to understand better existing mixing systems, and also the ability to evaluate mixer configurations computationally before undertaking costly experimental investigation. For example, alternate configurations of the Kenics mixer could be generated by varying the geometry of the mixer elements (length to diameter ratio, twist angle, etc.). The velocity fields for these alternate configurations could be obtained from CFD computations, and dynamical systems tools used to determine quantitatively the relative mixing performance for the different geometries. Moreover, these tools allow quantitative comparison of entirely different mixers. In addition, the Lagrangian tracking tools that have been developed could also be applied to other properties of interest for the flow system, such as heat or mass transfer, the aggregation and break-up of fluid drops, and chemical reactions.

Acknowledgements

This work was supported by awards to FJM from NSF (CTS 94-14460), from 3M, and from Dupont. DMH is grateful to Merck and Co., Inc. for support during the performance of this work.

Appendix A. Nomenclature

A	parameter representing the coefficient of variation of an unmixed stream (Eq. (4))
B	parameter representing the change in coefficient of variation vs. mixer length (Eq. (4))
C_i	concentration in sample i
$\bar{C}$	average concentration
D	mixer diameter
dA	cross-sectional area represented by each tracer particle
$\boldsymbol{F}$	deformation gradient tensor
$F(\theta)$	cumulative residence time distribution
$F'(\theta)$	area-weighted residence time distribution
$H_n(\log_{10}\lambda)$	probability density function of the logarithm of stretching values
$\boldsymbol{H}(\xi)$	rescaled value for $H_n(\log_{10}\lambda)$, defined in Eq. (12)
$\boldsymbol{I}$	identity tensor
$\boldsymbol{l}$	fluid filament vector tracked for stretching computations
$\boldsymbol{l}_0$	initial condition for vector $\boldsymbol{l}$
L	axial length of a single mixer element
N_i	number of tracer particles in sample i
$\bar{N}$	average number of particles per cell
n	period
Q_{in}	total inlet volumetric flow rate
R	mixer radius
Re	empty tube Reynolds number, $\mathrm{Re}=\frac{\rho\langle v_x\rangle D}{\mu}$
$\boldsymbol{x}$	vector of particle position (x, y, z)
$\boldsymbol{v}(\boldsymbol{x})$	particle velocity as a function of position
v_x, v_y, v_z	x-, y-, and z-components of fluid velocity
$\nabla\boldsymbol{v}$	velocity gradient
$\boldsymbol{x}$	vector of particle position (x, y, z)

Greek letters

α	specific stretching per period
Λ	mean of the logarithm of multipliers $\lambda_{j-1,j}$ for a single period
Λ_n	mean of $\log\lambda_{0,n}=\log_{10}\langle\lambda_g\rangle$
λ	stretching experienced by vector $\boldsymbol{l}$
$\lambda_{0,n}(i)$	stretching for particle i during the period from 0 to n
$\langle\lambda_g\rangle$	geometric average of stretching over all vectors on a given cross-section
μ	fluid viscosity
ρ	fluid density
θ	normalized residence time
σ^2	variance
σ	standard deviation
τ	residence time of a single tracer particle
ξ	short-time Lyapunov exponent, $\xi=(1/n)\log\lambda_{0,n}$

References

[1] H. Aref, Stirring by chaotic advection, J. Fluid Mech. 143 (1984) 1.
[2] H. Aref, S. Balachandar, Chaotic advection in a Stokes flow, Phys. Fluids 29 (1986) 3515.
[3] P.D. Swanson, J.M. Ottino, A comparative computational and experimental study of chaotic mixing of viscous fluids, J. Fluid Mech. 213 (1990) 227.
[4] F.J. Muzzio, P.D. Swanson, J.M. Ottino, The statistics of stretching and stirring in chaotic flows, Phys. Fluids A 3 (1991) 822.
[5] F.J. Muzzio, C. Meneveau, P.D. Swanson, J.M. Ottino, Scaling and multifractal properties of mixing in chaotic flows, Phys. Fluids A 4 (1992) 1439.

[6] F.J. Muzzio, P.D. Swanson, J.M. Ottino, Mixing distributions produced by multiplicative stretching in chaotic flows, Int. J. Bifurc. Chaos 2 (1992) 37.
[7] D.V. Khakhar, J.G. Franjione, J.M. Ottino, A case study of chaotic mixing in deterministic flows: the partitioned-pipe mixer, Chem. Eng. Sci. 42 (1987) 2909.
[8] H.A. Kusch, J.M. Ottino, Experiments on mixing in continuous chaotic flows, J. Fluid Mech. 236 (1992) 319.
[9] D.M. Hobbs, P.D. Swanson, F.J. Muzzio, Numerical characterization of low Reynolds number flow in the Kenics static mixer, to Chem. Eng. Sci. (1997) to appear.
[10] J. Arimond, L. Erwin, Modeling of continuous mixers in polymer processing, J. Eng. Ind. Trans. ASME 107 (1985) 70.
[11] J. Arimond, L. Erwin, A simulation of a motionless mixer, Chem. Eng. Commun. 37 (1985) 105.
[12] K. Dackson, E.B. Nauman, Fully developed flow in twisted tapes: a model for motionless mixing, Chem. Eng. Commun. 54 (1987) 381.
[13] F.H. Ling, X. Zhang, A numerical study on mixing in the Kenics static mixer, Chem. Eng. Commun. 136 (1995) 119.
[14] W.H. Press, B.P. Flannery, S.A. Teukolsky, W.T. Vetterling, Numerical Recipes (The Art of Scientific Computing), Cambridge University Press, Cambridge, 1986.
[15] T.T. Tung, Low Reynolds number entrance flows: a study of a motionless mixer, PhD Thesis, University of Massachusetts, 1976.
[16] P. Pustelnik, J. Petera, Residence time distribution of Ostwald–De Waele fluid in Kenics static mixer, 5th European Conf. on Mixing, Wurzburg, 1985, p. 407.
[17] P. Pustelnik, Investigation of residence time distribution in Kenics static mixers, Chem. Eng. Process. 102 (1986) 147.
[18] S.J. Chen, In-line, continuous mixing and processing of cosmetic products, J. Soc. Cosmet. Chem. 24 (1973) 639.
[19] S. Middleman, Fundamentals of Polymer Processing, McGraw-Hill, New York, 1977.
[20] Z. Tadmor, C.G. Gogos, Principles of Polymer Processing, Wiley, New York, 1979.
[21] C.D. Grace, Static mixing and heat transfer, Chem. Proc. Eng. (1971) 57.
[22] P.V. Danckwerts, The definition and measurement of some characteristics of mixtures, Appl. Sci. Res. A3 (1952) 279.
[23] P.T. Allocca, Mixing efficiency of static mixing units in laminar flow, Fiber Prod. (1982) 12.
[24] M.H. Pahl, E. Muschelknautz, Static mixers and their applications, Int. Chem. Eng. 22 (1982) 197.
[25] J.C. Godfrey, Static mixers, in: N. Harnby, M.F. Edwards, A.W. Nienow (eds.), Mixing in the Process Industries, Butterworth-Heinmann, Oxford, 1922, p. 225.
[26] V. Rom-Kedar, A. Leonard, S. Wiggins, An analytical study of transport, mixing and chaos in an unsteady vortical flow, J. Fluid Mech. 214 (1990) 347.
[27] D. Beigie, A. Leonard, S. Wiggins, A global study of enhanced stretching and diffusion in chaotic tangles, Phys. Fluids A 3 (1991) 1039.
[28] D. Beigie, A. Leonard, S. Wiggins, Statistical relaxation under nonturbulent chaotic flows: non-Gaussian high-stretch tails of finite-time Lyapunov exponent distributions, Phys. Rev. Lett. 70 (1993) 275.
[29] M. Liu, R.L. Peskin, F.J. Muzzio, C.W. Leong, Structure of the stretching field in chaotic cavity flows, AIChE J. 40 (1994) 1273.
[30] M. Liu, F.J. Muzzio, R.L. Peskin, Effects of manifolds and corner singularities on stretching in chaotic cavity flows, Chaos Sol. Fract. 4 (1994) 2145.